Translational and internal energy distributions of methyl and hydroxyl radicals produced by 157 nm photodissociation of amorphous solid methanol

Tetsuya Hama,[1] Masaaki Yokoyama,[1] Akihiro Yabushita,[1] Masahiro Kawasaki,[1,a)] Piyumie Wickramasinghe,[2] Wei Guo,[2] Hans-Peter Loock,[2] Michael N. R. Ashfold,[3] and Colin M. Western[3]

[1]*Department of Molecular Engineering, Kyoto University, Kyoto 615-8510, Japan*
[2]*Department of Chemistry, Queen's University, Kingston, Ontario K7L 3N6, Canada*
[3]*School of Chemistry, University of Bristol, Bristol BS8 1TS, United Kingdom*

(Received 7 July 2009; accepted 17 October 2009; published online 10 December 2009)

Methanol is typically observed within water-rich interstellar ices and is a source of interstellar organic species. Following the 157 nm photoexcitation of solid methanol at 90 K, desorbed $CH_3(v=0)$ and $OH(v=0,1)$ radicals have been observed *in situ*, near the solid surface, using resonance-enhanced multiphoton ionization (REMPI) detection methods. Time-of-flight and rotationally resolved REMPI spectra of the desorbed species were measured, and the respective fragment internal energy and kinetic energy distributions were obtained. Photoproduction mechanisms for CH_3 and OH radicals from solid methanol are discussed. The formation of $O(^1D$ and $^3P)$ atoms and H_2O was investigated, but the yield of these species was found to be negligible. CH_3 products arising following the photoexcitation of water-methanol mixed ice showed similar kinetic and internal energy distributions to those from neat methanol ice. © *2009 American Institute of Physics*. [doi:10.1063/1.3259877]

I. INTRODUCTION

Methanol is the smallest closed shell alcohol and has long served as a model for the dissociation of organic molecules. There is a comparably large body of literature on the vacuum ultraviolet (VUV) photolysis of methanol in the gas phase.[1–6] The results of the gas phase methanol photolysis studies at 157 nm showed that the relative contribution of the atomic hydrogen elimination process is larger than that of the molecular hydrogen elimination process, i.e., the ratio is 1:0.21.[2] C–O bond cleavage [reaction (1)] is another primary photoprocess following excitation of the $2\ ^1A''-X\ ^1A''$ transition in the 151–163 nm region, where it competes with the atomic and molecular hydrogen elimination processes,

$$CH_3OH + h\nu \rightarrow CH_3 + OH. \quad (1)$$

The relative contribution of the C–O bond cleavage channel in the gas phase photolysis at 157 nm has yet to be determined.[2,3] Reaction (1) was also observed following the photoexcitation of CH_3OH in various rare-gas matrices at 4 K and the photodissociation threshold energy for reaction (1) identified at $\lambda \sim 175$ nm.[7] Since methanol is known to be a component of the icy mantle on interstellar grains, comets, and other solar system bodies,[8–11] the effects of irradiating pure methanol ice by electrons, ions, and UV photons have each received much experimental study.[12–16]

Compared to the gas phase, however, the photochemical processes occurring in condensed phase samples of CH_3OH are more complicated because of the many possible secondary reactions on/in solid CH_3OH.[15,16] UV absorption of methanol in the condensed phase is observed at wavelengths shorter than the ~185 nm threshold.[17] Gerakines *et al.* reported VUV ($\lambda > 110$ nm) photolysis studies of solid CH_3OH at 10 K. Hydrogen (H_2), carbon monoxide (CO), carbon dioxide (CO_2), formyl radical (HCO), formaldehyde (H_2CO), methane (CH_4), and methyl formate (CH_3OCHO) were detected as products by *in situ* infrared (IR) absorption spectroscopy, but CH_3 and OH radicals were not.[16] CH_4 production from VUV photolysis of solid methanol was reported to scale linearly with irradiation time.[15,16] Unimolecular photodissociation,

$$CH_3OH + h\nu \rightarrow CH_4(X\ ^1A_1) + O(^1D), \quad (2)$$

is thus one plausible CH_4 formation mechanism. As Gerakines *et al.* noted, however, further research is necessary since gas phase photolysis studies have failed to reveal any evidence of reaction (2).[2,3,16]

To obtain a more complete mechanism understanding of amorphous solid methanol (ASM) photolysis—including possible secondary reactions on/in ASM—it would be helpful to determine the kinetic and internal energy distributions of the photoproducts generated from the primary photodissociation of ASM. Hama *et al.* previously used sensitive resonance-enhanced multiphoton ionization (REMPI) methods to determine the translational and internal energy distributions of, and thus formation mechanisms for, photodesorbed H atoms and H_2 molecules following VUV photolysis of ASM.[18]

In this paper, we investigate the mechanisms, the dynamics of production and the possible reactions of CH_3 and OH

a)Author to whom correspondence should be addressed. Electronic mail: kawasaki@moleng.kyoto-u.ac.jp. FAX: +81-75-383-257.

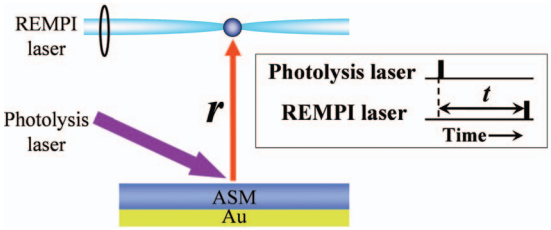

FIG. 1. Schematic illustration of the experiment. Photofragments from the 157 nm photodissociation of ASM are detected by the REMPI technique. The timing plot for measurements of a TOF spectrum is shown in the inset where the delay time t between photolysis and probe laser pulses corresponds to the TOF. r is the vertical distance between the disk substrate and the REMPI detection point. The VUV photoirradiated area is a disk with a radius of 6 mm.

products following 157 nm photodissociation of ASM at 90 K, using REMPI methods to determine their respective translational energy distributions and internal state population distributions. Possible secondary reactions on/in ASM are discussed in light of the obtained results. An attempt was also made to detect $O(^1D)$ and $O(^3P)$ atoms and H_2O products.

II. EXPERIMENTAL

A. Apparatus and preparation of ice films

The apparatus has been described before, and only details relevant to the present experiments are given here.[19] As shown in the schematic diagram of the experimental arrangement (Fig. 1), photodesorbed products were ionized at the focal point of the REMPI probe laser light, which was separated from the ice surface by a vertical distance of r. ASM was prepared by backfilling deposition of methanol vapor onto the gold substrate at 90 K for 60 min. The exposure was typically 1500 L (1 L$=1\times10^{-6}$ Torr s) to exclude the influence of reactions at the ASM/substrate interface.[20,21]

Since crystallization of solid methanol occurs at temperatures above 103.4 K, the morphology of the prepared solid methanol is amorphous.[22] Unfocused 157 nm laser (Lambda Physik, OPTexPro) radiation with a pulse duration of 10 ns [full width at half maximum (FWHM)] was incident on the ice surface at an angle of ~80° to the surface normal and at a fluence, $F<0.1$ mJ ($\sim10^{14}$ photons) cm^{-2} pulse^{-1}, which roughly corresponds to that in molecular clouds over $\sim10^4$ yr.[23] CH_3 photoproducts were ionized at a distance of $r=2$ mm from the substrate surface (4 mm for the case of OH products). CH_3 products were detected by (2+1) REMPI via the $4p_z\,^2A_2'(v'=0)\leftarrow X\,^2A_2''(v''=0)$ transition in the wavelength range of 285.0–287.0 nm and collected with a small mass spectrometer aligned perpendicular to the ice surface.[24] OH products were probed by (2+1) REMPI via the $D\,^2\Sigma^-(v'=0)\leftarrow X\,^2\Pi(v''=0)$ transition at 243.5–245.0 nm and via the $D\,^2\Sigma^-(v'=1)\leftarrow X\,^2\Pi(v''=0)$ and $3\,^2\Sigma^-(v'=0)\leftarrow X\,^2\Pi(v''=1)$ transitions in the wavelength range of 237.5–237.7 nm.[25] PGOPHER, a program for simulating rotational structure,[26] was used to simulate the measured spectra and thereby establish the product rotational temperatures. Detection of $O(^1D_2)$, $O(^3P_{J=2,1,0})$ atoms and H_2O molecules was attempted also by (2+1) REMPI via the $O(^1F_3\leftarrow{}^1D_2)$ transition at 203.8 nm, the $O(^3P_J-{}^3P_J)$ transition at 225.6–226.4 nm, and the $C(000)$-$X(000)$ transition at 247.3–248.6 nm, respectively,[27–29] but no signal was observed. Photodesorption of $O(^1D_2)$, $O(^3P_{J=2,1,0})$ atoms, and H_2O molecules has been previously observed with the same REMPI setup following the 157 nm photolysis of H_2O ice at 90 K.[29–31]

Recognizing that photoproducts might accumulate on the ASM surface after prolonged irradiation by 157 nm photolysis pulses, and that the photochemistry of these products might influence the measured product (state) distributions, the ASM surface was continually refreshed by intermissive exposure to CH_3OH vapor. In the present experiments, the pulsed valve was opened after each laser shot so as to deposit a fresh layer of ASM.

For the CH_3OH/H_2O codeposited ice photolysis experiments, CH_3OH/H_2O (1:1 mixture) vapor was deposited on the gold substrate. As before, the exposure was typically 1500 L and, again, fresh surfaces of cocondensed CH_3OH/H_2O were prepared as described above. All of the present photolysis experiments were performed at a sample temperature of 90 K, and the chamber pressure was 5×10^{-7} Torr (due to the intermissive CH_3OH or CH_3OH/H_2O vapor injection into the chamber).

B. Simulation of (2+1) REMPI spectra

CH_3 products were monitored by (2+1) REMPI via the $4p_z\,^2A_2''(v'=0)\leftarrow X\,^2A_2''(v''=0)$ transition. Spectral simulation employed the program PGOPHER (Ref. 26) and the spectroscopic constants reported by Black and Powis.[24] The $4p_z\,^2A_2''(v'=0)$ state predissociates with a level dependent efficiency.[24] This affects the measured REMPI line intensities and linewidths such that the latter vary as $\{0.4+0.08[N(N+1)-K^2]\}$ (in cm^{-1}), while the former declines by the square of this term. The measured spectra show evidence of power broadening also, which we accommodate by further broadening each transition with a Lorentzian function (3 cm^{-1} FWHM) and by reducing the relative weighting of the zero rank component of this two-photon transition. The two-photon transition probability is carried by two (a zero and a second rank) components. The former contributes only to the intense central Q branch (which is noticeably saturated under the present conditions), while the latter gives rise to O, P, Q, R, and S branches.

The REMPI features associated with OH products were also assigned and simulated using literature constants for the relevant electronic states.[25,32] The two-photon absorption cross sections reported by Greenslade *et al.*[25] allow estimation of the $(v''=1)/(v''=0)$ branching ratio in the OH products.

C. Simulation of time-of-flight spectra of photoproducts

Time-of-flight (TOF) spectra of the CH_3 and OH photoproducts were taken as a function of time t between the photolysis and REMPI laser pulses using a delay generator (Stanford Research) in order to investigate the flight times and thus translational energies of the desorbing photoprod-

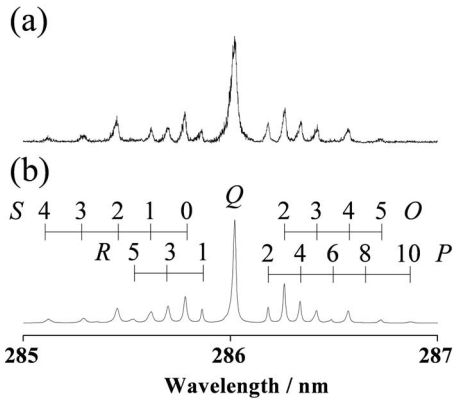

FIG. 2. (a) (2+1) REMPI excitation spectrum of CH_3 radicals from the 157 nm photolysis of a fresh ASM sample at 90 K, recorded at $t=6.0$ μs. (b) Simulated REMPI excitation spectrum of CH_3 radicals, resonance enhanced at the two photon energy by the $4p_z\ ^2A_2''(v'=0)$ level, assuming a Boltzmann distribution rotational state population distribution with $T_{rot}=150$ K.

ucts as shown schematically in Fig. 1. The measured TOF spectra, $S(a_i,t,T_{trans})$, of the CH_3 and OH products were fitted to a sum of one or more flux-weighted Maxwell–Boltzmann (MB) distributions, S_{MB}, each defined by a translational temperature, T_{trans}. Details regarding the simulation of such TOF spectra have been reported previously.[19] The coefficients, a_i, define the relative population associated with each MB component,

$$S(a_i,t,T_{trans})=\Sigma a_i S_{MB}(t,T_{trans}), \tag{3}$$

$$S_{MB}(t,T_{trans})=r^3t^{-4}\exp[-mr^2/2k_BT_{trans}t^2], \tag{4}$$

where r is the flight distance. The MB distribution, $P_{MB}(E_t)$, as a function of translational energy, E_t, is characterized by the averaged translational energy, $\langle E_t\rangle=2k_BT_{trans}$, where k_B is the Boltzmann constant,[33]

$$P_{MB}(E_t)=(k_BT_{trans})^{-2}E_t\exp[-E_t/k_BT_{trans}]. \tag{5}$$

Conversion from the E_t distribution to the TOF distribution was performed using the Jacobian listed by Zimmerman and Ho.[34]

In these calculations for details, we assume that signals come from a disk (VUV photoirradiation area) with a radius of 6 mm. Hence, an effective flight length is given by $(r^2+R^2)^{1/2}$ and the detection probability is proportional to $2\pi R dR/(r^2+R^2)$, where $r=2$ and 4 mm for the case of CH_3 and OH products, respectively, and $0\leqslant R\leqslant 6$ mm.[19] The variable R is the radius of the irradiation area which was defined in Ref. 19. For the angular distribution of the photofragments from the ice surface, $\cos^n\theta$, where θ is the surface polar coordinate, $n=0$ was adopted in the best-fitting procedures because the parent CH_3OH molecules adsorb randomly on the ASM surfaces.[19,35]

III. RESULTS

A. Kinetic energy and rotational energy distributions of the CH_3 radical

Figure 2(a) shows a rotationally resolved REMPI spectrum of $CH_3(v''=0)$ products formed following the 157 nm photolysis of freshly deposited ASM recorded at a fixed delay of $t=6.0$ μs. The spectrum is readily assignable to the $4p_z\ ^2A_2''(v'=0)\leftarrow X^2A_2''(v''=0)$ transition;[24,36] the best-fit simulation is shown in Fig. 2(b). The rotational temperature, T_{rot}, is estimated to be 150 ± 50 K ($\langle E_{rot}\rangle=1.2\pm0.4$ kJ mol^{-1}) by comparison with the spectral simulation. Figure 3 shows a typical TOF spectrum of the CH_3 products monitored at a REMPI wavelength of 286.0 nm (i.e., in the congested Q branch), which is reproduced well by a sum of two MB distributions with $T_{trans}=3000\pm1000$ K ($\langle E_{trans}\rangle=49.9\pm16.6$ kJ mol^{-1}) and 90 ± 20 K ($\langle E_{trans}\rangle=1.5\pm0.3$ kJ mol^{-1}). Table I summarizes these results. Changing the REMPI probe wavelength, e.g., to the $S(2)$ line at 285.45 nm, led to no appreciable change in the TOF profile. We were unable to characterize the rotational resolved REMPI spectrum for the $T_{trans}=3000$ K component in terms of a specific T_{rot} because of the weak signal intensity.

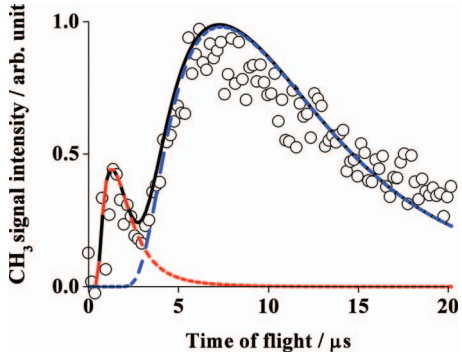

FIG. 3. TOF spectrum of CH_3 radicals from the 157 nm photolysis of a fresh ASM sample, monitoring on the Q branch of the (2+1) REMPI spectrum shown in Fig. 2. The solid curves are fits to the data derived assuming two MB distributions with $T_{trans}=3000$ K (10 %) and 90 K (90 %). The vertical flight distance used in these experiments is 2 mm.

B. Kinetic energy and rotational distributions of the OH radical

Figure 4(a) shows a rotationally resolved REMPI spectrum of the $OH(v=0)$ products recorded at $t=2.0$ μs, i.e., at the maximum of the single peak in their TOF spectrum. Spectral simulation [Fig. 4(b)] returns a best-fit rotational temperature $T_{rot}(v=0)=300$ K, and the rotational temperature $T_{rot}(v=0)$ is estimated to be 300 ± 100 K by spectral simulation ($\langle E_{rot}\rangle=2.5\pm0.8$ kJ mol^{-1}). Figures 5(a) and 5(b) show typical TOF spectra of the $OH(v=0)$ and $OH(v=1)$

TABLE I. Translational and rotational temperatures and energies of $CH_3(v=0)$ products.

Time-of-flight component, contributions	Translational energy E_T (kJ mol^{-1})	Rotational temperature T_{rot} (K)	Rotational energy E_R (kJ mol^{-1})
$CH_3(T_{trans}=3000$ K), 10%	49.9 ± 16.6	[a]	[a]
$CH_3(T_{trans}=90$ K), 90%	1.5 ± 0.3	150 ± 50[b]	1.2 ± 0.4[b]

[a]The rotational spectrum could not be characterized by a specific T_{rot} because of the weakness of the signal intensity.
[b]From spectra recorded at $t=6.0$ μs.

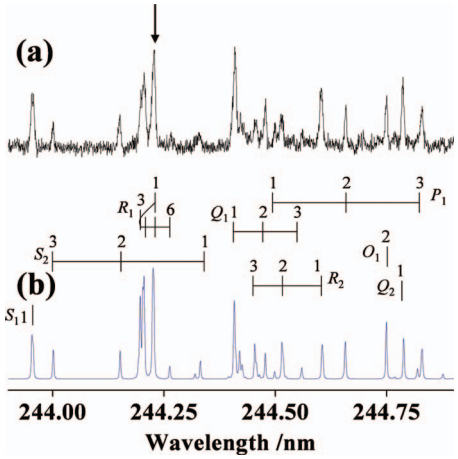

FIG. 4. (a) (2+1) REMPI excitation spectrum of OH radicals from the 157 nm photolysis of a fresh ASM sample at 90 K, recorded at $t=2.0$ μs. (b) Simulation of the $D\,^2\Sigma^- \leftarrow X\,^2\Pi(v'=0,v''=0)$ two-photon excitation spectrum of OH assuming a Boltzmann rotational state population distribution with $T_{rot}=300$ K. The arrow indicates the $R_1(1)+R_1(5)$ line used when measuring the TOF spectrum.

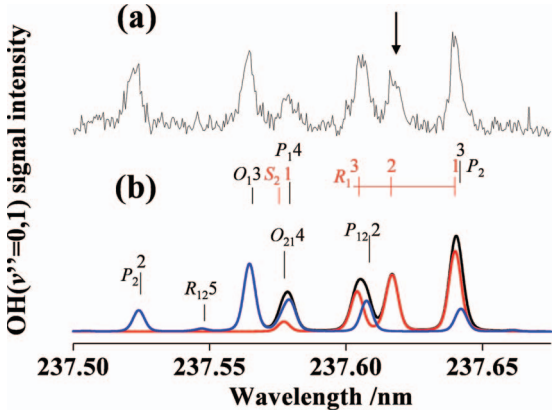

FIG. 6. (a) (2+1) REMPI excitation spectrum of OH radicals from the 157 nm photolysis of a fresh ASM sample at 90 K recorded at $t=2.0$ μs. (b) Simulation of relevant parts of the overlapping $D\,^2\Sigma^- \leftarrow X\,^2\Pi(v'=1,v''=0)$ and $3\,^2\Sigma^- \leftarrow X\,^2\Pi(v'=0,v''=1)$ two-photon transitions of OH assuming Boltzmann rotational state population distribution with $T_{rot}(v''=0)=300$ K (blue line) and $T_{rot}(v''=1)=200$ K (red line). The black line is the sum of the spectral simulations. The arrow indicates the $R_1(2)$ line used when measuring the TOF spectrum.

products monitoring, respectively, the $R_1(1)+R_1(5)$ line and the $R_1(2)$ line in the REMPI spectrum. Both are reproduced well by a single MB distribution with $T_{trans}=3000\pm500$ K ($\langle E_{trans}\rangle=49.9\pm8.3$ kcal mol^{-1}). No component with $T_{trans}=90$ K was detected, in contrast to CH_3 products. Figure 6(a) shows another portion of the OH REMPI spectrum which contains overlapping contributions from both OH($v=0$) and OH($v=1$) products, recorded at $t=2.0$ μs; the accompanying simulation [Fig. 6(b)] employs $T_{rot}(v=0)=300$ K and $T_{rot}(v=1)=200$ K. The rotational temperature $T_{rot}(v=1)$ is estimated to be 200 ± 50 K by spectral simulation ($\langle E_{rot}\rangle=1.7\pm0.4$ kJ mol^{-1}). The OH($v=1$)/OH($v=0$) population ratio is determined to be 0.2 ± 0.1. Table II summarizes these results.

C. Additional 157 nm photolysis experiments involving ASM

To assess possible contributions from secondary processes on the ASM surface and in the bulk, additional experiments were performed wherein TOF spectra of CH_3 and OH products formed by 157 nm photolysis of ASM were measured after 30 min photoirradiation without the intermissive dosing of CH_3OH vapor. No discernible differences were found in either the TOF spectra or the rotationally resolved REMPI spectra of the CH_3 or OH products recorded with the fresh or photoirradiated ASM samples. These results support the views that (a) the observed CH_3 and OH radicals are produced directly via the C–O cleavage reaction (1) and (b) secondary photoprocesses on/in ASM make no contribution to the formation of these desorbing species.

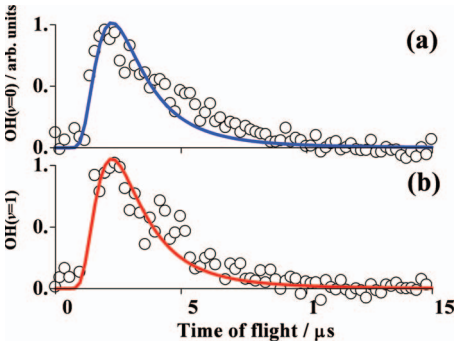

FIG. 5. TOF spectra of OH radicals from the 157 nm photolysis of a fresh ASM sample, obtained by monitoring (a) the $R_1(1)+R_1(5)$ line in the OH $D\,^2\Sigma^- \leftarrow X\,^2\Pi(v'=0,v''=0)$ two-photon transition and (b) the $R_1(2)$ line in the OH $3\,^2\Sigma^- \leftarrow X\,^2\Pi(v'=0,v''=1)$ two-photon transition. The solid curves are fits to the data derived assuming a MB translational energy distribution with $T_{trans}=3000$ K in both cases. The vertical flight distance used in these experiments is 4 mm.

REMPI signals attributable to O(^1D) and O(^3P) atoms were sought in the TOF range $0.5\ \mu s \leqslant t \leqslant 30\ \mu s$, but not observed. The primary formation of methane and O(^3P) products is a spin-forbidden process, i.e.,

$$CH_3OH + h\nu \rightarrow CH_4(X\,^1A_1) + O(^3P). \quad (6)$$

O(^1D) and O(^3P) atoms have been successfully detected with the same REMPI setup following the 157 nm photolysis of H_2O or H_2O_2 ices films at 90 K.[30,31] The lack of detectable O(^1D) and O(^3P) atoms in the present methanol experiments is in accord with the results of gas phase methanol photolysis studies at 157 nm (Refs. 2 and 3) and suggests that the primary formation of methane and O(^1D) or O(^3P) products via reactions (2) and (6) plays at most a minor role.

To verify that the measured CH_3 product state distributions are not affected by possible contamination from back-

TABLE II. Translational and rotational temperatures and energies of OH($v=0$ and 1) products.

	OH($v=0$)		OH($v=1$)[a]	
	Translation	Rotation	Translation	Rotation
Temperature (K)	3000 ± 500	300 ± 100[b]	3000 ± 500	200 ± 50[b]
Energy (kJ mol^{-1})	49.9 ± 8.3	2.5 ± 0.8	49.9 ± 8.3	1.7 ± 0.4

[a]Population ratio OH($v=1$)/OH($v=0$)$=0.2\pm0.1$.
[b]From spectra recorded at $t=2.0$ μs.

ground water vapor, the ASM sample was changed to a 1:1 mixture of CH_3OH/H_2O ice. The intensities of the $T_{trans}=3000$ and 90 K components of the CH_3 radical TOF signal from the mixed sample were both reduced, and the majority of the CH_3 products are accommodated to the substrate temperature (90 K) which was similar to that from pure, fresh ASM samples.

A similar check is not possible for the OH products because of the contribution from OH products formed by simultaneous photolysis of H_2O.[37,38]

IV. DISCUSSION

The C–O bond cleavage has been observed as a primary process following photolysis of CH_3OH both in the gas phase and in solid rare-gas matrices,[2,3,7]

$$CH_3OH(ads) + h\nu \rightarrow CH_3(i) + OH(i), \quad \Delta H = 422.6 \text{ kJ mol}^{-1}. \tag{7}$$

The available energy for reaction (7) at 157 nm ($E_{phot}=757.3$ kJ mol^{-1}) is $E_{avail}(7)=334.7$ kJ mol^{-1}, calculated using liquid phase thermodynamic data for the condensed or adsorbed species ("ads") and gas phase data for species on the ASM/vacuum interface ("i").[39,40] The center of mass kinetic energy distribution of the CH_3 and OH products resulting from 157 nm photolysis of gas phase CH_3OH shows maximum probability at 217.6 kJ mol^{-1} and extends to 372.4 kJ mol^{-1}, which is consistent with the gas phase value for $E_{avail}(7)$.[2,3] This translational energy is partitioned between the CH_3 and OH fragments according to momentum conservation, such that the most probable fragment translational energies are, respectively, 117.2 and 100.4 kJ mol^{-1}. These values are much higher than those found in the present condensed phase study with $E_{avail}(7)=334.7$ kJ mol^{-1}, wherein we determine an average center of mass translational energy for the photodesorbed CH_3 and OH products of only 99.6 kJ mol^{-1}. This reduced partitioning of $E_{avail}(7)$ into product translational energy could be due to cage effects and the dissipation of available energy into the ASM bulk.[7,17]

Hama *et al.* performed direct measurements of photodesorbed hydrogen atoms and molecules following VUV photolysis of amorphous solid CH_3OH and CD_3OH.[18] The results showed that H and D atoms are produced via reactions (8) and (9),

$$CD_3OH + h\nu \rightarrow CD_3O + H, \tag{8}$$

$$CD_3OH + h\nu \rightarrow CD_2OH + D. \tag{9}$$

Highly vibrationally excited D_2 and $HD(v=2-5)$ molecules were also produced as primary products by unimolecular elimination from methanol, i.e., reactions (10) and (11),

$$CD_3OH + h\nu \rightarrow CDOH + D_2(v=2-5), \tag{10}$$

$$CD_3OH + h\nu \rightarrow CD_2O + HD(v=2-5). \tag{11}$$

Reactions (8)–(11) and the C–O bond cleavage (7) are the primary photodissociation processes of ASM. However, the branching ratio of the primary photoprocesses could not be quantified either in our previous or the present studies.

No IR absorption signal attributable to CH_3 and OH radicals was observed in earlier VUV photolysis studies of solid methanol at 10 K.[15,16] These results imply that (a) the quantum yield of the C–O bond cleavage reaction (7) on the surface under VUV irradiation is small or, (b) CH_3 and OH photoproducts, if formed, are removed by photodesorption and reactions on/in ASM and thus remain undetected. In the following sections, possible secondary reactions of CH_3 and OH products on/in ASM are proposed.

A. CH_3 radical formation in the 157 nm photolysis of fresh ASM

Two MB components, characterized by $T_{trans}=3000$ and 90 K and with respective relative yields of 10% and 90%, are required to fit the TOF spectrum of CH_3 products measured at 157 nm. The CH_3 rotational temperatures for the $T_{trans}=90$ K component are almost thermally equilibrated with the substrate temperature (90 K), as shown in Table I. Since 90% of the CH_3 fragments are accommodated to the substrate temperature, and the translational and rotational energies are much lower than $E_{avail}(7)$, we propose that the majority of the nascent CH_3 products are formed by absorption in the ASM bulk and are subsequently relaxed by collisions within the ASM *en route* to the vacuum. Only a small fraction (10%) of the CH_3 products are produced at the exposed ASM surface and retain a high translational temperature, i.e.,

$$CH_3OH + h\nu \rightarrow CH_3(T_{trans}=3000 \text{ K}) + OH, \tag{12}$$

$$CH_3(3000 \text{ K}) \xrightarrow{\text{collision}} CH_3(90 \text{ K}). \tag{13}$$

CH_3 photoproducts may also be removed by reactions within the bulk and thereby remain undetected by IR absorption spectroscopy.[15,16] For example, hydrogen abstraction from methanol by CH_3 radicals, reactions (14) and (15), are known in the gas phase,[41]

$$CH_3(i) + CH_3OH(ads) \rightarrow CH_4(i) + CH_2OH(i), \quad \Delta H = 4.2, \quad E_a = 58.6 \text{ kJ mol}^{-1}, \tag{14}$$

$$CH_3(i) + CH_3OH(ads) \rightarrow CH_4(i) + CH_3O(i), \quad \Delta H = 33.5, \quad E_a = 56.9 \text{ kJ mol}^{-1}. \tag{15}$$

The quoted activation energies, E_a, are *ab initio* estimates from MP2 and MP4 calculations reported by Jodkowski *et al.*[41] Some of the CH_3 products formed at the ASM/vacuum interface with $\langle E_{trans}\rangle=49.8$ kJ mol^{-1} and considerable internal energy may have sufficient energy to induce the H abstraction reactions (14) and (15) but, as Table I shows, most of the CH_3 photoproducts relax to $T_{trans}=90\pm20$ K and $T_{rot}=150\pm50$ K. At this stage, their average energy ($\sim$2.7 kJ mol^{-1}) is far too small to overcome such activation barriers. The thermally equilibrated CH_3 photoproducts then diffuse through the bulk ASM until they desorb from the solid/vacuum interface.

Other possible removal processes for CH_3 include (generally barrierless) reaction with other radical photoproducts, e.g., reaction with H-atom photoproducts to form methane,

$$CH_3(i) + H(i) + M \rightarrow CH_4(i) + M, \quad \Delta H = -439.3 \text{ kJ mol}^{-1}. \tag{16}$$

Compared to the gas phase, we might anticipate a significant enhancement in the rate of reaction (16) in ASM since H atoms are very mobile, even at low temperature, and reaction (16) is a highly exothermic, three-body reaction. H atoms are known to be present in high density following pulsed 157 nm laser excitation of ASM at 90 K, and H_2 molecule formation from H atoms has also been reported,[18] i.e.,

$$CH_3OH + h\nu \rightarrow CH_2OH/CH_3O + H, \tag{17}$$

$$H + CH_3OH \rightarrow CH_2OH/CH_3O + H_2(v = 0 \text{ and } 1), \tag{18}$$

$$H + H \rightarrow H_2(v \geqslant 2). \tag{19}$$

Earlier VUV photolysis studies of solid methanol at 10 K found the yield of CH_4 to depend linearly on the irradiation time, but no IR absorption signal attributable to CH_3 was observed,[15,16] probably because these radicals were efficiently consumed by reaction with H atoms, i.e., via reaction (16).

In the mixed CH_3OH/H_2O ice experiment, the TOF signal intensity of the CH_3 radicals was reduced. This may be due to (a) the reduction in CH_3OH density on the surface, or (b) the reaction of CH_3 products with H atoms or OH radicals formed from photolysis of H_2O. The reaction of CH_3 with water molecules is unlikely: the TOF profile of CH_3 radicals produced from the mixed ice showed a similar behavior to that from the fresh ASM samples, i.e., the majority of the CH_3 products are accommodated to the substrate temperature (90 K). This implies that the CH_3 products desorb without reaction with solid water, as would be expected given the large activation energy of reaction (20),

$$CH_3(i) + H_2O(ads) \rightarrow CH_4(i) + OH(i), \quad \Delta H = 104.6, \quad E_a = 138.1 \text{ kJ mol}^{-1}. \tag{20}$$

The activation energy or reaction (20) was estimated from theoretical calculations for the reverse process, $CH_4 + OH \rightarrow CH_3 + H_2O$, by Bravo-Pérez *et al.*[42]

The translational temperatures of the photodesorbed H or OH products following the 157 nm photolysis of water ice have been previously observed with the same REMPI setup.[38,43,44] The previous results showed that the majority of the photodesorbed H atoms were relaxed by collisions within the water ice and the translational temperature was accommodated to the substrate temperature. The photodesorbed OH radicals, on the other hand, were not thermally equilibrated with the substrate temperature but were likely formed near the water ice surface, whereas collisionally cooled OH products were either efficiently trapped in the bulk or reacted with water.[38,43,44]

B. OH radical formation in the 157 nm photolysis of fresh ASM

The translational energies of $OH(v=0 \text{ and } 1)$ products from the 157 nm photolysis of fresh ASM are described by a single temperature $T_{trans} = 3000 \pm 500$ K ($\langle E_{trans} \rangle = 49.9 \pm 8.3$ kJ mol^{-1}). The OH rotational temperatures, $T_{rot}(v=0) = 300 \pm 100$ K and $T_{rot}(v=1) = 200 \pm 50$ K, are not thermally equilibrated with the substrate temperature of 90 K, as shown in Table II. These results suggest that (a) the observed $OH(v=0 \text{ and } 1)$ fragments originate from the ASM surface, not the bulk, and (b) $OH(v=0 \text{ and } 1)$ radicals formed in the ASM bulk are either efficiently trapped or react in the bulk as described before in the 157 nm photolysis of H_2O,[37,38] i.e.,

$$CH_3OH + h\nu \rightarrow CH_3 + OH(T_{trans} = 3000 \text{ K}), \tag{21}$$

$$OH(3000 \text{ K}) \xrightarrow{\text{collision}} \text{trapped or react with ASM}. \tag{22}$$

Possible H abstraction reactions from methanol by OH radicals are

$$OH(i) + CH_3OH(ads) \rightarrow H_2O(i) + CH_2OH(i), \quad \Delta H = -50.2, \quad E_a = 3.8 \text{ kJ mol}^{-1}, \tag{23}$$

$$OH(i) + CH_3OH(ads) \rightarrow H_2O(i) + CH_3O(i), \quad \Delta H = -25.1, \quad E_a = 14.6 \text{ kJ mol}^{-1}. \tag{24}$$

The activation energies quoted are for the corresponding gas phase reactions, estimated by Jodkowski *et al.*[41] Reaction (23) has been proposed previously in methanol-water condensed phase systems.[45] Recalling Table II, the OH products from the 157 nm photolysis of ASM have ample energy to overcome the barriers for reactions (23) and (24), and thus OH radical initiated hydrogen abstraction is likely to occur on/in ASM.

However, neither photodesorption nor production of H_2O was observed in either the present or earlier VUV photolysis studies on ASM.[15,16] These results imply that the yield of OH production via the C–O bond cleavage reaction (7) on the surface is small and that the secondary H_2O formation via reactions (23) and (24) does not proceed efficiently.

C. Other possible secondary reactions

After photolysis of a CH_3OH molecule in bulk ASM, the probability of reaction (25) is expected to be high since the photogenerated CH_3 and OH radicals are effectively caged by the ASM matrix,[17,46,47] i.e.,

$$CH_3(i) + OH(i) + M \rightarrow CH_3OH(ads) + M, \quad \Delta H = -422.6 \text{ kJ mol}^{-1}, \tag{25}$$

the bimolecular reaction between gas phase CH_3 and OH radicals has been studied extensively, both theoretically and experimentally.[48] The calculations of Jasper *et al.* show a number of reactive radicals and molecular products from this

reaction, e.g., CH_3OH, $HCOH+H_2$, and CH_2+H_2O.[48] In the condensed phase, Hodyss *et al.* reported a UV (130–335 nm) photolysis study of CH_4-H_2O ice mixtures at 20 K.[49] Their analysis assumes that OH radicals formed by the photodissociation of water react with methane to form CH_3 radicals, which then recombine with OH radicals to form methanol.

Ethane formation, from the recombination reaction of two CH_3 radicals [reaction (26)], was also reported in the photolysis of CH_4-H_2O ice mixtures,[49]

$$CH_3(i) + CH_3(i) + M \rightarrow C_2H_6(i) + M, \quad \Delta H = -376.6 \text{ kJ mol}^{-1}. \tag{26}$$

No IR absorption attributable to C_2H_6 was observed in the earlier VUV photolysis studies of solid CH_3OH at 10 K, however.[15,16] This finding is understandable if CH_3 photoproducts react with other species (e.g., H, OH, or CH_3OH) much more frequently than they encounter another CH_3 radical.

Hodyss *et al.*[49] proposed that the presence of CH_4 in CH_4-H_2O ice mixtures inhibited the formation of H_2O_2 (from the combination of two OH radicals) by serving as a trap for OH radicals, since the C–H bonds are also attacked by OH radicals. In fact, no IR absorption features attributable to H_2O_2 or OH were observed in the VUV photolysis of solid CH_3OH at 10 K.[15,16] Our previous experimental work has confirmed that OH radicals are formed following the 157 nm photolysis of H_2O_2 photoproducts on the ASW surface as well as by primary photolysis of surface H_2O, and that the translational energy of OH radicals from H_2O_2 was much larger than that from H_2O.[38] There are no discernible differences in the TOF spectra, or the rotational resolved REMPI spectra, of the OH radicals from the 157 nm photolysis of fresh or photoirradiated ASM samples, i.e., the OH radicals detected in the present study are produced directly, via reaction (7), and not from secondary photolysis of photogenerated H_2O_2.

V. CONCLUSION

The translational and rotational temperatures of $CH_3(v=0)$ and $OH(v=0$ and 1) radicals (i.e., the products from the primary C–O bond cleavage) have been measured following pulsed 157 nm irradiation of ASM at 90 K. Most of the detected CH_3 species have low translational and internal energies, implying that these photoproducts accommodate to the ASM bulk temperature and desorb from the ASM surface without reaction in the bulk near the solid/vacuum interface. The detected OH fragments, in contrast, are deduced to originate exclusively from the ASM surface; any OH radicals formed in the ASM bulk phase are readily trapped or react in the bulk phase. The equivalence of the TOF spectra of CH_3 fragments from ASM and from a mixed CH_3OH-H_2O ice sample indicates that the reactivity of solid water with CH_3 products is small.

ACKNOWLEDGMENTS

This work was supported by a Grant-in-Aid from JSPS (Grant No. 20245005). M.K. and M.N.R.A. remain very grateful for the award of a Daiwa-Adrian prize that facilitated earlier phases of this collaboration. P.W., W.G., and H.P.L. acknowledge financial support from the Natural Sciences and Engineering Research Council of Canada.

[1] S. Harich, J. J. Lin, Y. T. Lee, and X. Yang, J. Chem. Phys. **111**, 5 (1999).
[2] S. Harich, J. J. Lin, Y. T. Lee, and X. Yang, J. Phys. Chem. A **103**, 10324 (1999).
[3] S. H. Lee, H. I. Lee, and Y. T. Lee, J. Chem. Phys. **121**, 11053 (2004).
[4] Y. Wen, J. Segall, M. Dulligan, and C. Wittig, J. Chem. Phys. **101**, 5665 (1994).
[5] S. Pilling, R. Neves, A. C. F. Santos, and H. M. Boechat-Roberty, Astron. Astrophys. **464**, 393 (2007).
[6] S. Satyapal, J. Park, R. Bersohn, and B. J. Katz, J. Chem. Phys. **91**, 6873 (1989).
[7] B.-M. Cheng, C.-P. Liu, W.-J. Lo, and Y.-P. Lee, Nucl. Instrum. Methods Phys. Res. A **467**, 1461 (2001).
[8] K. M. Pontoppidan, E. Dartois, E. F. van Dishoeck, W. F. Thi, and L. d'Hendecourt, Astron. Astrophys. **404**, L17 (2003).
[9] M. J. Mumma, M. A. DiSanti, K. Magee-Sauer, B. P. Bonev, G. L. Villanueva, H. Kawakita, N. D. Russo, E. L. Gibb, G. A. Blake, J. E. Lyke, R. D. Campbell, J. Aycock, A. Conrad, and G. M. Hill, Science **310**, 270 (2005).
[10] D. P. Cruikshank, T. L. Roush, M. J. Bartholomew, T. R. Geballe, Y. J. Pendleton, S. M. White, J. F. Bell III, J. K. Davies, T. C. Owen, C. de Bergh, D. J. Tholen, M. P. Bernstein, R. H. Brown, K. A. Tryka, and C. M. Dalle Ore, Icarus **135**, 389 (1998).
[11] D. P. Cruikshank, T. L. Roush, and F. Poulet, C. R. Phys. **4**, 783 (2003).
[12] C. J. Bennett, S.-H. Chen, B.-J. Sun, A. H. H. Chang, and R. I. Kaiser, Astrophys. J. **660**, 1588 (2007).
[13] G. A. Baratta, G. Leto, and M. E. Palumbo, Astron. Astrophys. **384**, 343 (2002).
[14] G. A. Baratta, A. C. Castorina, G. Leto, M. E. Palumbo, F. Spinella, and G. Strazzulla, Planet. Space Sci. **42**, 759 (1994).
[15] W. A. Schutte and P. A. Gerakines, Planet. Space Sci. **43**, 1253 (1995).
[16] P. A. Gerakines, W. A. Schutte, and P. Ehrenfreund, Astron. Astrophys. **312**, 289 (1996).
[17] Y.-P. Kuo, H.-C. Lu, Y.-J. Wu, B.-M. Cheng, and J. F. Ogilvie, Chem. Phys. Lett. **447**, 168 (2007).
[18] T. Hama, M. Yokoyama, A. Yabushita, and M. Kawasaki, J. Chem. Phys. **130**, 164505 (2009).
[19] A. Yabushita, Y. Inoue, T. Senga, M. Kawasaki, and S. Sato, J. Phys. Chem. B **106**, 3151 (2002).
[20] N. G. Petrik and G. A. Kimmel, J. Phys. Chem. C **113**, 4451 (2009).
[21] N. G. Petrik, A. G. Kavetsky, and G. A. Kimmel, J. Chem. Phys. **125**, 124702 (2006).
[22] S. M. Dounce, J. Mundy, and H. L. Dai, J. Chem. Phys. **126**, 191111 (2007).
[23] A. Yabushita, T. Hama, D. Iida, N. Kawanaka, M. Kawasaki, N. Watanabe, M. N. R. Ashfold, and H.-P. Loock, Astrophys. J. **682**, L69 (2008).
[24] J. F. Black and I. Powis, J. Chem. Phys. **89**, 3986 (1988).
[25] M. E. Greenslade, M. I. Lester, D. C. Radenovic, A. J. A. van Roij, and D. H. Parker, J. Chem. Phys. **123**, 074309 (2005).
[26] C. M. Western, PGOPHER, a program for simulating rotational structure, University of Bristol, available at http://pgopher.chm.bris.ac.uk.
[27] S. T. Pratt, P. M. Dehmer, and J. L. Dehmer, Phys. Rev. A **43**, 4702 (1991).
[28] Y. Matsumi, N. Shafer, K. Tonokura, M. Kawasaki, Y.-L. Huang, and R. J. Gordon, J. Chem. Phys. **95**, 7311 (1991).
[29] A. Yabushita, T. Hama, M. Yokoyama, M. Kawasaki, S. Andersson, R. N. Dixon, M. N. R. Ashfold, and N. Watanabe, Astrophys. J. **699**, L80 (2009).
[30] T. Hama, A. Yabushita, M. Yokoyama, M. Kawasaki, and N. Watanabe, J. Chem. Phys. **131**, 114510 (2009).
[31] T. Hama, A. Yabushita, M. Yokoyama, M. Kawasaki, and N. Watanabe, J. Chem. Phys. **131**, 114511 (2009).
[32] K. P. Huber and G. Herzberg (data prepared by J. W. Gallagher and R. D. Johnson, III), "Constants of Diatomic Molecules," in NIST Chemistry

WebBook, NIST Standard Reference Database Number 69, P. J. Linstrom and W. G. Mallard, National Institute of Standards and Technology, Gaithersburg, MD, 20899, see http://webbook.nist.gov/ (retrieved 2009).
[33] F. M. Zimmermann and W. Ho, J. Chem. Phys. **100**, 7700 (1994).
[34] F. M. Zimmermann and W. Ho, Surf. Sci. Rep. **22**, 127 (1995).
[35] A. Yabushita, Y. Inoue, T. Senga, M. Kawasaki, and S. Sato, J. Phys. Chem. A **108**, 438 (2004).
[36] P. Quintana, R. F. Delmdahl, D. H. Parker, B. Martinez-Haya, F. J. Aoiz, L. Banares, and E. Verdasco, Chem. Phys. Lett. **325**, 146 (2000).
[37] A. Yabushita, T. Hama, D. Iida, and M. Kawasaki, J. Chem. Phys. **129**, 014709 (2008).
[38] T. Hama, A. Yabushita, M. Yokoyama, M. Kawasaki, and S. Andersson, J. Chem. Phys. **131**, 054508 (2009).
[39] M. Kh. Karapet'yants and M. K. Karapet'yants, *Handbook of Thermodynamic Constants of Inorganic and Organic Compounds* (Ann Arbor-Humphrey Science, London, 1970).
[40] S. P. Sander, R. R. Friedl, A. R. Ravishankara, D. M. Golden, C. E. Kolb, M. J. Kurylo, M. J. Molina, G. K. Moortgat, H. Keller-Rudek, B. J. Finlayson-Pitts, P. H. Wine, R. E. Huie, and V. L. Orkin, Chemical Kinetics and Photochemical Data for Use in Atmospheric Studies Evaluation No. 15 (2006).
[41] J. T. Jodkowski, M.-T. Rayez, J.-C. Rayez, T. Bérces, and S. Dóbé, J. Phys. Chem. A **103**, 3750 (1999).
[42] G. Bravo-Pérez, J. R. Alvarez-Idaboy, A. G. Jiménez, and A. Cruz-Torres, J. Chem. Phys. **310**, 213 (2005).
[43] A. Yabushita, Y. Hashikawa, A. Ikeda, M. Kawasaki, and H. Tachikawa, J. Chem. Phys. **120**, 5463 (2004).
[44] A. Yabushita, D. Kanda, N. Kawanaka, M. Kawasaki, and M. N. R. Ashfold, J. Chem. Phys. **125**, 133406 (2006).
[45] M. C. Akin, N. G. Petrik, and G. A. Kimmel, J. Chem. Phys. **130**, 104710 (2009).
[46] S. Andersson, A. Al-Halabi, G.-J. Kroes, and E. F. van Dishoeck, J. Chem. Phys. **124**, 064715 (2006).
[47] S. Andersson and E. F. van Dishoeck, Astron. Astrophys. **491**, 907 (2008).
[48] A. W. Jasper, S. J. Klippenstein, L. B. Harding, and B. Ruscic, J. Phys. Chem. A **111**, 3932 (2007).
[49] R. Hodyss, P. V. Johnson, J. V. Stern, J. D. Goguen, and I. Kanik, Icarus **200**, 338 (2009).